Coarse-graining microscopic strains in a harmonic, two-dimensional solid: Elasticity, nonlocal susceptibilities, and nonaffine noise

K. Franzrahe* and P. Nielaba
Fachbereich Physik, Universität Konstanz, Postfach 692, 78457 Konstanz, Germany

S. Sengupta
Centre for Advanced Materials, Indian Association for the Cultivation of Science, Jadavpur, Kolkata 700 032, India and Advanced Materials Research Unit, Satyendra Nath Bose National Centre for Basic Sciences, Block-JD, Sector-III, Salt Lake, Kolkata 700 098, India

(Received 7 August 2009; revised manuscript received 16 June 2010; published 22 July 2010)

In soft matter systems the local displacement field can be accessed directly by video microscopy enabling one to compute local strain fields and hence the elastic moduli in these systems using a coarse-graining procedure. We study this process in detail for a simple triangular, harmonic lattice in two dimensions. Coarse-graining local strains obtained from particle configurations in a Monte Carlo simulation generates nontrivial, nonlocal strain correlations (susceptibilities). These may be understood within a generalized, Landau-type elastic Hamiltonian containing up to quartic terms in strain gradients [K. Franzrahe *et al.*, Phys. Rev. E **78**, 026106 (2008)]. In order to demonstrate the versatility of the analysis of these correlations and to make our calculations directly relevant for experiments on colloidal solids, we systematically study various parameters such as the choice of statistical ensemble, presence of external pressure and boundary conditions. Crucially, we show that special care needs to be taken for an accurate application of our results to actual experiments, where the analyzed area is embedded within a larger system, to which it is mechanically coupled. Apart from the smooth, affine strain fields, the coarse-graining procedure also gives rise to a *noise* field (χ) made up of *nonaffine* displacements. Several properties of χ may be rationalized for the harmonic solid using a simple "cell model" calculation. Furthermore the scaling behavior of the probability distribution of the *noise* field (χ) is studied. We find that for any inverse temperature β, spring constant f, density ρ and coarse-graining length Λ the probability distribution can be obtained from a master curve of the scaling variable $\mathcal{X}=\chi\beta f/\rho\Lambda^2$.

DOI: 10.1103/PhysRevE.82.016112 PACS number(s): 62.20.F−, 62.20.D−, 82.70.Dd, 05.10.Ln

I. INTRODUCTION

Soft matter with its structural and elastic properties offers an attractive route to the design of new materials. In particular colloidal dispersions attract a lot of interest in this context. Surface chemistry or alterations in the composition of the solvent give an excellent control over the effective interactions in colloidal dispersions [1]. By definition colloids lie in the range of the visible spectrum. Video microscopy [2] is therefore a straightforward means to gain information of the microscopic trajectories of the components of the system under study. Thus, microscopic, thermal (or Brownian) fluctuations can be resolved directly in real space, making colloidal dispersions excellent model systems for the study of fundamental questions of the statistical physics of soft condensed matter. Two-dimensional colloidal dispersions, for example, have been used successfully in studies on melting in two dimensions during the last decades [3–6]. In this paper, we focus on the mechanical properties of such systems and consider how they may be obtained from the microscopic particle trajectories.

Within linear elasticity (e.g., [7]), a solid in two dimensions is described by eight unknown variables: the three stresses σ_{ij}, three strains ϵ_{ij} and two components of the displacement field u_i. Appropriately, there are also eight equations, namely the two equilibrium conditions $\partial\sigma_{ji}/\partial x_j+f_i=0$ (with f_i, the forces per unit volume within the body), three geometrical equations $\epsilon_{ij}=(\partial u_i/\partial x_j+\partial u_j/\partial x_i)/2$, and three constitutive equations $\sigma_{ij}=C_{ijkl}\epsilon_{kl}$. This set of equations may be solved for a given boundary condition in order to extract either the stresses or strains, given the elastic moduli. If by contrast the strains are known for a given stress configuration or vice versa, the elastic moduli themselves can be calculated. This manner of obtaining elastic moduli would require us to perturb the system using some external means, e.g., laser tweezers [8]. In contrast to this approach, one may also calculate the tensor of elastic constants C_{ijkl} of a system from fluctuations of the microscopic strains obtained by a coarse-graining procedure. We follow this second approach, as computing C_{ijkl} in this way requires *no* external forces to be applied. This is one of the advantages of the approach, as external forces might change the very properties that are being measured [9–12]. Another advantage is that the interaction potential of the particles need not be known. Recently, this procedure was further extended in Ref. [13] to obtain even the nonlocal elastic susceptibilities.

We intent to establish a precise procedure for obtaining mechanical properties from microscopic configuration data. In addition, we aim to study in some detail fundamental aspects of the coarse-graining procedure, which is employed in the calculation of the nonlocal susceptibilities. In this present paper, we concentrate on the following three points: (1) We present in detail, how elastic moduli and correlation lengths

*kerstin.franzrahe@uni-konstanz.de

can be obtained from the nonlocal elastic susceptibilities. (2) We discuss the impact of various parameters on the nonlocal elastic susceptibilities and their interpretation. For example different choices of statistical ensemble, changes in the boundary conditions or system size are considered. (3) The coarse-graining procedure itself and the nonaffinity it gives rise to are studied.

One aspect of point (2) we want to emphasize is that an embedding medium influences the relations between the nonlocal susceptibilities and the elastic constants. This is often the case in experimental systems, if only a subvolume of the lattice is accessible to the analysis. The proper interpretation of the correlation functions in such settings and the importance of finite-size effects are discussed. This shows how the analysis has to be adapted to the actual experimental situation and facilitates the adoption of such techniques for routine analysis of experimental data

In the context of point (3) aspects to consider are for example the presence of particle configurations within the coarse-graining volume, which are not describable in terms of affine deformations of any reference lattice, e.g., incipient vacancy-interstitial pairs. This is true for all coarse-graining volumes larger than a unit cell. What is the effect of these configurations on elasticity? How do they influence mechanical behavior? A study of these fluctuations in ideal solids, as presented in Sec. IV, may help us understand complex dynamics in solids better.

The organization of this paper together with a short summary of our main results is as follows. In Sec. II, we derive an analytic form of the nonlocal elastic response function, or compliance $\chi_{ij}(\vec{r},\vec{r}')$ $(i=x,y)$. It is defined as the strain $\varepsilon_{ij}(\vec{r}')$ produced at position $\vec{r}'$ due to a stress $\sigma_{ij}(\vec{r})$ at $\vec{r}$. To this end, we consider a Landau expansion [14] of the free energy in terms of the strains, keeping up to quartic terms in the gradients and derive an analytic form of the two-point correlation functions G_{ij}. These are related to the response function via $\chi_{ij}=(k_BT)^{-1}G_{ij}$. For a homogeneous solid without external load (i.e., $\langle\varepsilon_i(\vec{r})\rangle=0$) the correlation functions are given by $G_{ij}(\vec{r}')=V\langle\varepsilon_i(\vec{0})\varepsilon_j(\vec{r}')\rangle$. The $\langle\cdots\rangle$ denote a thermal average (and in addition one over the choice of origin) and k_BT is the Boltzmann constant times the temperature. In Sec. III, we present Monte Carlo computer simulations of a harmonic crystal. The calculation of the local strain field corresponds to a coarse-graining procedure and allows us to construct the strain-strain correlation functions G_{ij} from simulation data. We compare our results, obtained for a variety of ensembles and boundary conditions to that of the Landau theory. A common feature in experimental systems is the presence of an embedding medium, surrounding the analyzed region of the sample. The effects of such an embedding medium on the strain correlations are discussed and visualized by use of a statistical sum rule. Section IV discusses the origin of one of our significant results: though the forms of the correlation functions and their limiting values as predicted by the Landau theory are reproduced, the G_{ij} obtained from simulations through our coarse-graining procedure differ by an additional background contribution which is not negligible. We argue that this is a consequence of nonaffine displacements, which are not considered in the ansatz for the Landau theory. We analyze the nonaffineness χ. Its probability distribution $P(\chi)$ shows well defined scaling properties with the spring stiffness f and the coarse-graining length Λ. The autocorrelation function for χ is shown to be short ranged decaying rapidly for distances much larger than the coarse-graining length. Finally, we conclude our paper indicating future directions for research.

II. LANDAU THEORY FOR THE STRAINS

In soft matter systems microscopic, thermal fluctuations can be resolved directly in real space. Thus the local displacements $\vec{u}$, as they are carried by individual particles, are directly accessible. In order to describe such a system as an elastic continuum, we need to coarse grain the discrete displacement fields of individual particles over some predetermined coarse graining length. As a result of the coarse-graining fluctuations of the strains with wavelength smaller than the coarse-graining length are not considered in the analysis of such systems. The elastic Hamiltonian describing the two-dimensional elastic continuum is given below.

$$\beta\mathcal{H}_0=\frac{1}{2}\int d\vec{r}C_{ijkl}\epsilon_{ij}\epsilon_{kl}. \tag{1}$$

In order to be able to extract information on the elastic properties of a system from the knowledge of the fluctuations of the local displacements $\vec{u}$ we formulate a Landau theory in the strains. Classical, linear elasticity theory assumes that the strains are purely affine. Within the framework of Landau theory formulas for the two-point correlation functions can be derived.

Some of the formalism used in the presented derivation of nonlocal susceptibilities is similar to that used for deriving the equilibrium structure of droplet fluctuations of Martensitic products within a parent austenite matrix, see for example the following references and references therein [15]. Note however that here we employ the formalism to demonstrate how information on elastic properties of a *one-phase* solid can be obtained from the study of the nonlocal elastic susceptibilities.

We start from the following, dimensionless ansatz for the Landau functional [13,14,16]:

$$\beta\mathcal{F}=\frac{1}{2}\int d^2x\sum_{i=1}^{3}\{a_ie_i^2+c_i(\nabla e_i)^2+c_i'(\nabla^2e_i)^2\}. \tag{2}$$

Here with $(i=1-3)$ the dimensionless constants a_i are the elastic moduli of the system, while c_i and c_i' are phenomenological coefficients and the three strains e_i are given by $e_1=\epsilon_{xx}+\epsilon_{yy}$, describing pure volume changes; $e_2=\epsilon_{xx}-\epsilon_{yy}$, describing deviatoric shear strains and $e_3=\frac{1}{2}(\epsilon_{xy}+\epsilon_{yx})$, describing pure shear strains. The phenomenological coefficients c_i have the dimension of a length^2. Thus we interpret $\xi_{el,i}\sim\sqrt{c_i}$ as a correlation length. Note that unless stated otherwise throughout the paper all lengths are given in units of a, the lattice parameter of the underlying triangular lattice in the simulated systems.

The terms quadratic in the strains e_i represent the local part in this ansatz. Nonlocal contributions are included via the gradient terms. Note that the Landau functional Eq. (2)

should be strictly valid for excitations of wavelengths longer than a short-wavelength cutoff. In this analytic ansatz short wavelength excitations are suppressed by the gradient terms [14,16]. We have ignored the possibility of defects.

For nonuniform strains, spatial fluctuations of the strains couple and only one of the strain variables e_i in this ansatz is an independent variable. This can be seen as follows: all forces within and on the system must cancel for the system to be in thermodynamic equilibrium, i.e., $\frac{\partial \sigma_{ij}}{\partial x_j}=0$ for a solid under zero external stress; the case of external hydrostatic stress is presented in Sec. III C The stress tensor σ_{ij} can be obtained directly from Eq. (2), as $\sigma_{ij}=\frac{\delta \beta \mathcal{F}}{\delta \epsilon_{ij}}$. For a two-dimensional crystal this condition reads in Fourier space:

$$k_x a_1 \tilde{e}_1 + k_x a_2 \tilde{e}_2 + k_y a_3 \tilde{e}_3 = 0, \tag{3}$$

$$k_y a_1 \tilde{e}_1 - k_y a_2 \tilde{e}_2 + k_x a_3 \tilde{e}_3 = 0. \tag{4}$$

In addition, St. Venant's compatibility condition $\nabla \times (\nabla \times \epsilon)^T = 0$ (e.g., [7,17]) must be considered in the calculations, which ensures an unique relation between the displacement field $\vec{u}$ and the strain fields ϵ_{ij}. For a two-dimensional crystal it simplifies to

$$-k^2 \tilde{e}_1 + (k_x^2 - k_y^2)\tilde{e}_2 + 4k_x k_y \tilde{e}_3 = 0 \tag{5}$$

in Fourier space. These relations may now be used to eliminate any two of the strains from Eqs. (3)–(5) and obtain a free energy functional only in terms of the single remaining independent strain. The strain variables are related via the kernels $\tilde{Q}_{ij}$ to each other: $\tilde{e}_i = \tilde{Q}_{ij}\tilde{e}_j$. In detail we obtain:

$$\tilde{e}_2 = -\left(\frac{4a_1 + 2a_3}{a_1 + a_2}\right)\left(\frac{k_x k_y}{k_x^2 - k_y^2}\right)\tilde{e}_3 = \tilde{Q}_{23}\tilde{e}_3,$$

$$\tilde{e}_1 = -\left(\frac{2a_3 - 4a_2}{a_1 + a_2}\right)\left(\frac{k_x k_y}{k^2}\right)\tilde{e}_3 = \tilde{Q}_{13}\tilde{e}_3,$$

$$\tilde{e}_1 = \left(\frac{a_3 - 2a_2}{2a_1 + a_3}\right)\left(\frac{k_x^2 - k_y^2}{k^2}\right)\tilde{e}_2 = \tilde{Q}_{12}\tilde{e}_2.$$

Note that the properties of the correlation functions are set by the wave vector dependence of the kernels $\tilde{Q}_{ij}$.

We shall also need kernels relating the strains e_i to the local, microscopic rotations given by the antisymmetric part of the strain tensor $\theta = (\partial u_y/\partial x - \partial u_x/\partial y)/2$. Local rotations θ are related to the deviatoric strains e_2 and the pure shear strains e_3. Starting from the definitions of the strain variables the partial derivative $\partial^3\theta/\partial x^2 \partial y$ can be expressed solely in terms of e_2, e_3, and θ. Thus one obtains the following relation between the three shear strain variables in Fourier space:

$$\tilde{\theta}(k_x^2 + k_y^2) = (k_x^2 - k_y^2)\tilde{e}_3 - k_x k_y \tilde{e}_2.$$

We may now derive a new kernel relating $\tilde{\theta}$ to, e.g., the pure shear strain $\tilde{e}_3$ using the previously derived kernel $\tilde{Q}_{23}$. This results in:

$$\tilde{e}_3 = \frac{k_x^4 - k_y^4}{(k_x^2 - k_y^2)^2 + k_x^2 k_y^2\left(\frac{4a_1 + 2a_3}{a_1 + a_2}\right)}\tilde{\theta} = \tilde{Q}_{3\theta}\tilde{\theta}.$$

As the considerations in Sec. III D will show, it will be helpful to define the strain variable $e_{2\theta}=2\theta$. We will analyze its two-point correlation function in embedded systems, such as the colloidal crystal discussed in [13].

Appropriate for a comparison with our analysis of simulation data, we switch to a discretized notation on a square mesh. This facilitates the numerical calculation of Fourier transforms in the data analysis. Thus we have $e_1(\vec{x}) \to e_{1,\vec{m}}$ and $\vec{x} \to \vec{R}_{\vec{m}}$. Here $\vec{m}$, which is a tuple of integer lattice indices, specifies the position on the square mesh. In this notation the free energy can be rewritten as,

$$\beta\mathcal{F} = \frac{v_z}{2}\sum_{\vec{m}}\sum_{i=1}^{3}[a_i e_{i,\vec{m}}^2 + c_i(\nabla e_{i,\vec{m}})^2 + c_i'(\nabla^2 e_{i,\vec{m}})^2].$$

Here $v_z = V_z/a^2$ is the dimensionless volume of the square mesh cell and the summation runs over all N cells. Now one may use the above relations to finally express $\beta\mathcal{F}$ as a harmonic functional of only one of the strain components. This allows the direct calculation of the analytic form of the two-point correlation functions, as the partition function factorizes (see e.g., [18] for details). Here we choose as an example the strains $\tilde{e}_1$ and obtain the following expression for the functional, written as a sum over the wave vectors:

$$\beta\mathcal{F} = \frac{1}{2v}\sum_{\vec{k}}\{a_1 + k^2 c_1 + k^4 c_1' + (a_2 + c_2 k^2 + c_2' k^4)[\tilde{Q}_{21}(\vec{k})]^2 + (a_3 + c_3 k^2 + c_3' k^4)[\tilde{Q}_{31}(\vec{k})]^2\}\tilde{e}_{1,\vec{k}}\tilde{e}_{1,\vec{k}}^*$$

with $v = V/a^2$, the dimensionless volume of the system. It is now straight forward to calculate the two-point correlation function. We start from its general definition and take into account the fact, that the average strains $\langle e_i(\vec{r})\rangle$ in a crystal, which is under no load, is zero. So for the example, the strains e_1, we have

$$G_{11}(\vec{r},\vec{r}') = \langle e_1(\vec{r})e_1(\vec{r}')\rangle - \langle e_1(\vec{r})\rangle\langle e_1(\vec{r}')\rangle = \frac{1}{v^2}\sum_{\vec{k}\vec{k}'} e^{i((\vec{k}\cdot\vec{r})+(\vec{k}'\cdot\vec{r}'))}\langle \tilde{e}_{1,\vec{k}}\tilde{e}_{1,\vec{k}'}\rangle.$$

The explicit calculation of $\langle \tilde{e}_{1,\vec{k}}\tilde{e}_{1,\vec{k}'}\rangle$ making use of the given Landau functional yields the following relation:

$$\langle \tilde{e}_{1,\vec{k}}\tilde{e}_{1,\vec{k}'}\rangle = \delta_{\vec{k}+\vec{k}',\vec{0}}\langle|\tilde{e}_{1,\vec{k}}|^2\rangle = \frac{\delta_{\vec{k}+\vec{k}',\vec{0}}v}{a_1 + k^2 c_1 + k^4 c_1' + \sum_{j=2}^{3}(a_j + c_j k^2 + c_j' k^4)[\tilde{Q}_{j1}(\vec{k})]^2}.$$

With this result one can now write down the analytic form of the strain-strain correlation function in Fourier space, as in Fourier space the expression for the strain-strain correlation function simplifies to $\tilde{G}_{11}(\vec{k}) = \langle|\tilde{e}_{1,\vec{k}}|^2\rangle/v$. Analytic formulas for the remaining strain-strain correlation functions (viz., e_2,

e_3, and $e_{2\theta}$) were derived using analogous calculations [13]. For $i=1,2,3$ the structure of the strain-strain correlation functions is the same, while for $i=2\theta$ it differs slightly:

$$\tilde{G}_{ii}(\vec{k}\neq\vec{0}) = 1 \Big/ \left\{ a_i + k^2 c_i + k^4 c_i' + \sum_{j\neq i, j=1}^{3} (a_j + c_j k^2 + c_j' k^4)[\tilde{Q}_{ji}(\vec{k})]^2 \right\}, \tag{6a}$$

$$\tilde{G}_{ii}(\vec{0}) = 1/a_i,$$

$$\tilde{G}_{2\theta 2\theta}(\vec{k}\neq\vec{0}) = 1 \Big/ \left\{ \left[a_3 + c_3 k^2 + c_3' k^4 + \sum_{j=1}^{2} (a_j + c_j k^2 + c_j' k^4)(\tilde{Q}_{j3})^2 \right] (\tilde{Q}_{3\,2\theta})^2 \right\}, \tag{6b}$$

$$\tilde{G}_{2\theta 2\theta}(\vec{0}) = 4/a_3.$$

Properties of the strain-strain correlation functions

The analytic strain-strain correlation functions $\tilde{G}_{ii}(\vec{k})$ given in Eq. (6) are plotted in Fig. 1. The set of parameters a_i, c_i, and c_i' used in Fig. 1 were obtained from Monte-Carlo simulations in the *NVT* ensemble with periodic boundary conditions of a harmonic triangular lattice, to be discussed in Sec. III B While the deviatoric and shear strain correlation functions $\tilde{G}_{22}$ and $\tilde{G}_{33}$ have fourfold symmetries, the correlation function of the dilatation $\tilde{G}_{11}$ has an eightfold symmetry. The correlation functions may be interpreted as the response of the system to a localized perturbation at the origin. This perturbation is either a dilatation, a deviatoric shear or a pure shear. The resulting deformation of the solid may be decomposed into a superposition of the eigenmodes of the system. The eigenmodes for a square box, are plane waves with polarization either longitudinal or transverse to the coordinate axes with the eigenfrequencies forming a discrete spectrum: $\omega_{nm}=\frac{2\pi}{L}c_\alpha\sqrt{n^2+m^2}$ with $n,m\in N_0$. Thus, the wave vector of the eigenmodes along the diagonals, i.e., ($n=m$ or $n=-m$) as well as those along the coordinate axis ($n\neq 0$ and $m=0$ or $n=0$ and $m\neq 0$), exhibits a fourfold degeneracy. All remaining eigenmodes with $n\neq m\neq 0$ have an eightfold degeneracy. If the local perturbation at the origin is a dilatation, the resulting local deformation is a superposition of eigenmodes with four-as well as eightfold degeneracy. This leads to the eightfold rotational symmetry visible for the strain correlation function $\tilde{G}_{11}$. In contrast to this the two possible shear perturbations will excite elastic waves that are superpositions of *exclusively* eigenmodes with fourfold degeneracy. For this reason the corresponding correlation functions $\tilde{G}_{22}$ and $\tilde{G}_{33}$ exhibit only a fourfold rotational symmetry.

As was discussed in [19], the presence of defects, breaks the rotational symmetries of the strain correlation functions.

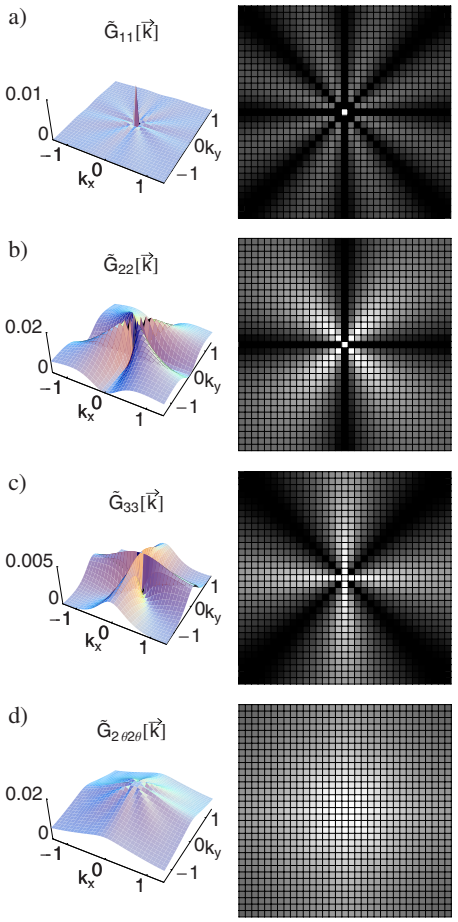

FIG. 1. (Color online) The analytic form of the strain-strain correlation functions. For each function a surface plot and next to it a density plot are shown. In the density plot the maxima are white, minima are black. The set of parameters used for plotting was obtained from a Monte Carlo simulation of a harmonic triangular lattice in the *NVT* ensemble with periodic boundary conditions: $a_1=97.4$, $a_2=48.1$, $a_3=198.2$, $c_1=54.3$, $c_2=37.4$, $c_3=118.2$, $c_1'=-86.1$, $c_2'=-1.3$, and $c_3'=-18.8$. (a) $G_{11}(\vec{k})$, (b) $G_{22}(\vec{k})$, (c) $G_{33}(\vec{k})$, and (d) $G_{2\theta 2\theta}(\vec{k})$.

The details of the structure of the correlation functions are dominated by the dependence of the kernels $\tilde{Q}_{ij}$ on the wave vector $\vec{k}$, especially for the cases $k_x=k_y$, $k_x\to 0$ while $k_y\neq 0$ and $k_y\to 0$ while $k_x\neq 0$. In particular, we obtain the following relations:

$$\tilde{Q}_{12} = \begin{cases} 0 & \text{for } k_x = k_y \\ -\left(\dfrac{a_3-2a_2}{2a_1+a_3}\right) & \text{for } k_x\to 0,\ k_y\neq 0 \\ \left(\dfrac{a_3-2a_2}{2a_1+a_3}\right) & \text{for } k_y\to 0,\ k_x\neq 0, \end{cases}$$

$$\tilde{Q}_{13} = \begin{cases} \left(\dfrac{2a_2-a_3}{a_1+a_2}\right) & \text{for } k_x = k_y \\ 0 & \text{for } k_x\to 0,\ k_y\neq 0 \\ 0 & \text{for } k_y\to 0\ k_x\neq 0, \end{cases}$$

$$\tilde{Q}_{23} = \begin{cases} \infty & \text{for } k_x = k_y \\ 0 & \text{for } k_x \to 0,\ k_y \neq 0 \\ 0 & \text{for } k_y \to 0,\ k_x \neq 0. \end{cases}$$

For the kernel $\tilde{Q}_{3\ 2\theta}$ relating e_3 to $e_{2\theta}$ the behavior along the specific directions in Fourier space for $\vec{k} \to \vec{0}$ can be extracted from the behavior of the correlation function $\tilde{G}_{33}(\vec{k})$ and $\tilde{G}_{22}(\vec{k})$. Along the coordinate axis the kernel relating $\tilde{e}_3$ to $\tilde{e}_{2\theta}$ becomes a constant,

$$\tilde{Q}_{3\ 2\theta} = \begin{cases} -1/2 & \text{for } k_x \to 0,\ k_y \neq 0 \\ 1/2 & \text{for } k_y \to 0,\ k_x \neq 0. \end{cases}$$

Thus the continuous behavior of the correlation function $\tilde{G}_{33}(\vec{k})$ for $\vec{k} \to \vec{0}$ *along* the coordinate axis carries over to the correlation function $\tilde{G}_{2\theta 2\theta}(\vec{k})$. The behavior along the diagonals $k_x = k_y$ can be extracted from the behavior of the product of the kernels $\tilde{Q}_{23}^2 \tilde{Q}_{3\ 2\theta}^2$, which can be shown to equal 1. Upon insertion of these relations into the equations for the correlation functions their behavior for these limiting cases can be extracted:

$$\tilde{G}_{11}(\vec{k}) = \begin{cases} 0, & k_x = k_y \neq 0 \\ 0, & k_x \to 0,\ k_y \neq 0 \\ 0, & k_y \to 0,\ k_x \neq 0, \end{cases}$$

$$\tilde{G}_{22}(\vec{k}) = \begin{cases} 1/[a_2 + c_2 k^2 + c_2' k^4], & k_x = k_y \neq 0 \\ 0, & k_x \to 0,\ k_y \neq 0 \\ 0, & k_y \to 0,\ k_x \neq 0, \end{cases}$$

$$\tilde{G}_{33}(\vec{k}) = \begin{cases} 0, & k_x = k_y \neq 0 \\ 1/[a_3 + c_3 k^2 + c_3' k^4], & k_x \to 0,\ k_y \neq 0 \\ 1/[a_3 + c_3 k^2 + c_3' k^4], & k_y \to 0,\ k_x \neq 0, \end{cases}$$

$$\tilde{G}_{2\theta 2\theta}(\vec{k}) = \begin{cases} 1/[a_2 + c_2 k^2 + c_2' k^4], & k_x = k_y \neq 0 \\ 4/[(a_3 + c_3 k^2 + c_3' k^4)], & k_x \to 0,\ k_y \neq 0 \\ 4/[(a_3 + c_3 k^2 + c_3' k^4)], & k_y \to 0,\ k_x \neq 0. \end{cases}$$

These considerations show, that in certain directions in Fourier space the shear strain variables become independent from each other and the corresponding correlation functions are continuous for $\vec{k} \to \vec{0}$. These are the directions, along which a fit will give direct access to the elastic constants and correlation lengths of the system.

Figure 2 shows cuts in Fourier space which correspond to these specific directions for the strain correlation functions $\tilde{G}_{ii}(\vec{k})$. For the correlation function of the pure shear strain $\tilde{G}_{22}(\vec{k})$ a cut along the diagonals is shown, while for the deviatoric strain correlation function $\tilde{G}_{33}(\vec{k})$ a cut along the coordinate axis is shown. The strain correlation function for the dilatation $\tilde{G}_{11}(\vec{k})$ in contrast is not continuous for $\vec{k} \to \vec{0}$. If one considers for example the direction $k_y = 2k_x$ the kernels $\tilde{Q}_{ij}$ relating the strain variables turn into constant weighting factors: $\tilde{Q}_{21} = -(\frac{2a_1+a_3}{a_3-2a_2})(\frac{5}{3})$ and $\tilde{Q}_{31} = (\frac{a_1+a_2}{4a_2-2a_3})(\frac{5}{2})$. Thus along

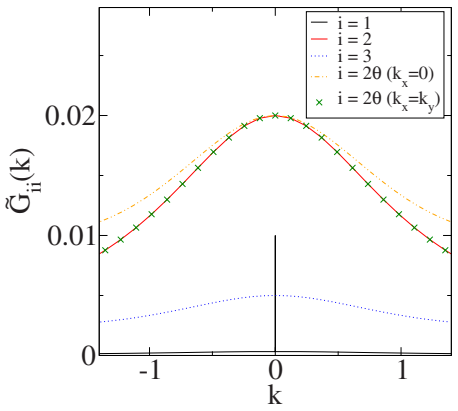

FIG. 2. (Color online) Cuts of the analytic strain-strain correlation functions along specific directions in Fourier space. The set of parameters used for plotting is: $a_1 = 100$, $a_2 = 50$, $a_3 = 200$ and $c_1 = 54.3$, $c_2 = 37.4$, $c_3 = 118.2$, $c_1' = -86.1$, $c_2' = -1.3$, and $c_3' = -18.8$. The correlations lengths were obtained from a Monte Carlo simulation of a harmonic triangular lattice in the *NVT* ensemble with periodic boundary conditions. $\tilde{G}_{11}(\vec{k})$ is shown along the direction $k_y = 2k_x$, $\tilde{G}_{22}(\vec{k})$ along the diagonal $k_x = k_y$, $\tilde{G}_{33}(\vec{k})$ along the k_y axis and $\tilde{G}_{2\theta 2\theta}(\vec{k})$ along the diagonal $k_x = k_y$ and along the k_y-axis.

the direction $k_y = 2k_x$ the strain correlation function for the dilatation $\tilde{G}_{11}(\vec{k})$ for $\vec{k} \to \vec{0}$ is given by

$$\tilde{G}_{11}(\vec{k} \to \vec{0}) = 1 \Bigg/ \left(a_1 + a_2 \left[-\left(\frac{2a_1 + a_3}{a_3 - 2a_2} \right) \left(\frac{5}{3} \right) \right]^2 + a_3 \left[\left(\frac{a_1 + a_2}{4a_2 - 2a_3} \right) \left(\frac{5}{2} \right) \right]^2 \right)$$
$$\neq \tilde{G}_{11}(\vec{k} = \vec{0}) = 1/a_1.$$

So the strain correlation function for the dilatation $\tilde{G}_{11}(\vec{k})$ exhibits a pronounced discontinuity for $\vec{k} \to \vec{0}$. In order to illustrate this fact, consider the set of parameters used in the simulations of a harmonic triangular lattice in Sec. III The choice of the spring constant sets the elastic constants of the system under consideration to $a_1 = 100$, $a_2 = 50$ and $a_3 = 200$. For $\vec{k} \to \vec{0}$ one has $\tilde{G}_{11}^{-1}(\vec{k} \to \vec{0}) \approx 3025$, which is approximately 30 times as much as the value for $\vec{k} = \vec{0}$, i.e., $\tilde{G}_{11}^{-1}(\vec{k} = \vec{0}) = a_1 = 100$, set by the bulk modulus—showing that nonuniform dilatations tend to be severely penalized in this solid.

Nevertheless, provided that the value of the bulk modulus is determined e.g., from $\tilde{G}_{11}(\vec{k} = \vec{0})$ the coefficients c_1 and c_1' can also be obtained by fitting one of the correlation functions along a cut in Fourier space. So in principle all 9 parameters of the free energy functional can be determined from an analysis of the strain-strain correlation functions. Like the correlation function of the dilatation $\tilde{G}_{11}(\vec{k})$, the correlation function of the microscopic rotations $\tilde{G}_{2\theta 2\theta}(\vec{k})$ shows an eightfold rotational symmetry. Unlike $\tilde{G}_{11}(\vec{k})$, however, $\tilde{G}_{2\theta 2\theta}(\vec{k})$ is continuous for $\vec{k} \to \vec{0}$ along the coordinate axis and the diagonal (compare Fig. 2). Therefore, fits along

these directions can be used to determine the elastic constants a_2 and a_3 as well as the coefficients c_2, c_2' and c_3, c_3'.

We shall next discuss the results of a coarse-graining procedure, which attempts to obtain these correlation functions and therefore the parameters of the Landau free energy functional from Monte Carlo simulations of the harmonic lattice. The coefficients of all the second and fourth order terms involving gradients of strain are found to be nonvanishing showing that coarse-graining generates these higher order nonlocal terms in the free energy.

III. MONTE CARLO SIMULATIONS OF A HARMONIC CRYSTAL

The analysis of a harmonic crystal is convenient for a comparison with the results of the Landau theory presented in the last section, since the elastic moduli can be directly calculated from the spring constants. We consider a harmonic triangular lattice with a Hamiltonian $\mathcal{H}=k_BT(f/2)\Sigma_{m,n=1}^{N}(|\vec{r}_m-\vec{r}_n|-a)^2$ where f is the spring constant and a the lattice parameter of the triangular lattice. The elastic moduli are related to the spring constant f via: $K=a_1=(\sqrt{3}/2)f$, $\mu=a_2=(\sqrt{3}/4)f$ and $4\mu=a_3=\sqrt{3}f$. Furthermore the harmonic triangular lattice has been shown to be a successful model for the interpretation of experiments on colloidal crystals [20]. It is modeled by N point particles each of them hard wired by spring constants f to the six nearest neighbors. We have carried out Monte Carlo simulations in the constant NpT and NVT ensembles with periodic boundary conditions. We also mention briefly results for a system with open boundary conditions which were presented elsewhere [13]. Next the influence of hydrostatic pressure is analyzed by Monte Carlo simulations in the constant NpT ensembles with periodic boundary conditions. Finally we consider the effect of a surrounding elastic medium and finite size effects in order to make contact with experiments on colloids.

The knowledge of the configurations and the reference lattice allows for a direct calculation of the displacement field $\vec{u}(\vec{r})$. In order to calculate the corresponding strain field partial differentials of the displacement field have to be calculated. We follow the procedure by Falk and Langer [21] and calculate the strain field by minimizing the error in the affine transformation that relates the actual configuration $\{\vec{r}\}$ to the reference lattice $\{\vec{R}\}$.

$$\vec{r}=\vec{R}+\vec{u}(\vec{R})=(\mathbf{1}+\boldsymbol{\epsilon})\vec{R}.$$

The mean-squared error in this mapping χ is thus a measure of how well the given situation can be described within the framework of linear elasticity theory. It quantifies the nonaffinity of the given displacement field. Falk and Langer [21] analyzed the temporal development of strains. We use an analogous definition for χ in thermodynamic equilibrium and evaluate the strains and nonaffineness with respect to the reference lattice:

$$\chi(\vec{r}_0)=\sum_{m=1}^{N_B}\sum_{i=1}^{2}\left(r_m^i-r_0^i-\sum_{j=1}^{2}(\delta_{ij}+\epsilon_{ij})[R_m^j-R_0^j]\right)^2. \quad (7)$$

Here $\vec{r}_0$ is the position, at which the strains are to be calculated, and N_B is the number of neighboring particles considered. This corresponds to a coarse-graining procedure, in which N_B is set by the choice of coarse-graining length Λ, i.e., cutoff radius within which particles are considered in the calculation. For the results presented in this section, we have used a cutoff radius of $\Lambda=1.3$ resulting in $N_B=6$. In Sec. IV we present some systematics showing how some of our results depend on the coarse-graining length Λ.

As mentioned above we map the triangular lattice to a square mesh in the calculation of the strain-strain correlation functions. This facilitates the numerical Fourier transformation of the calculated real space correlation functions. The wave vectors are limited to the first Brillouin zone, i.e., $k_j \in [-\frac{\pi}{l_m},\frac{\pi}{l_m}]$, with $j=x,y$. Here l_m represents the lattice parameter of the square mesh. Care must be taken in the choice of l_m to keep the mesh volume large enough so that artifacts due to the discreteness of the triangular lattice (and insufficient averaging) are avoided. In most of the results presented here we used $l_m=2.25a$, where a is the lattice parameter of the original, triangular lattice. Lastly, one also needs to be careful about correcting for global rotations and translations of the lattice so as not to introduce artificial sources of error.

Simulations of the harmonic triangular lattice were done for three system sizes $N=3120$, 4736, and 5822. We first discuss the results for simulations with spring constant $\beta a^2 f=200/\sqrt{3}$ in the NpT ensemble with periodic boundary conditions (and external pressure $\beta a^2 p=0$) and the NVT ensemble with periodic boundary conditions.

A. *NpT* ensemble with periodic boundary conditions

For the simulations of the harmonic crystal in the NpT ensemble we use the algorithm of Parinello and Rahman [22]. Here, the information on the actual shape of the simulation volume, which is free to fluctuate in this ensemble, is saved in the transformation matrix $\mathbf{h}$. One of the advantages of this implementation is, that from the fluctuations of the transformation matrix $\mathbf{h}$ the fluctuations of the strain tensor can be calculated directly. The strain tensor is related to the transformation matrix via [22]:

$$\boldsymbol{\epsilon}=\frac{1}{2}(\mathbf{h}_0^{T,-1}\mathbf{G}\mathbf{h}_0^{-1}-\mathbf{1}),$$

where $\mathbf{h}_0$ is the transformation matrix of the reference lattice and $\mathbf{G}=\mathbf{h}^T\mathbf{h}$ contains the information of the actual shape of the simulation volume. Table I shows a comparison of the elastic moduli for the harmonic, triangular lattice as they are expected for the chosen spring constant f and the values as they are obtained from the simulations in the NpT ensemble by analyzing the fluctuations of the simulation volume.

Figure 3 shows the strain-strain correlation functions in Fourier space as they are obtained from the simulations in the NpT ensemble with periodic boundary conditions. The comparison with the analytic predictions (Fig. 1) shows, that the eightfold rotational symmetry in $\tilde{G}_{11}(\vec{k})$ is not resolved. The shear strain correlation functions show clearly a fourfold rotational symmetry, as was expected from the analytic predictions.

Cuts along various directions in Fourier space of these functions are plotted in Fig. 4 for three system sizes. As these

TABLE I. A comparison of the elastic constants as calculated from the spring constant f and as obtained by use of various methods from data of a Monte Carlo simulation of a harmonic triangular lattice with $N=3120$ particles in the NpT ensemble at zero hydrostatic pressure $\beta a^2 p=0.0$ and spring constant $\beta a^2 f=200/\sqrt{3}$.

	a_1	a_2	a_3
Calculated from f	$100/\beta a^2$	$50/\beta a^2$	$200/\beta a^2$
From fluctuations of **h**	$98.9/\beta a^2$	$49.4/\beta a^2$	$196.7/\beta a^2$
From $\tilde{G}(\vec{k}=\vec{0})$	$96.8/\beta a^2$	$48.6/\beta a^2$	$190.8/\beta a^2$
From fits of $\tilde{G}(\vec{k}\neq\vec{0})$		$49.1/\beta a^2$	$195.7/\beta a^2$

cuts show, there is no systematic dependence on the system size in the correlation functions.

The discontinuities in the correlation functions are visible in Figs. 3 and 4. Nevertheless the extreme discontinuity one expected for $\tilde{G}_{11}(\vec{k})$ from the analytic predictions is reduced to a factor of approximately 1.5 instead of 30. This can be clearly seen by comparing the cuts in Figs. 2 and 4(a). This

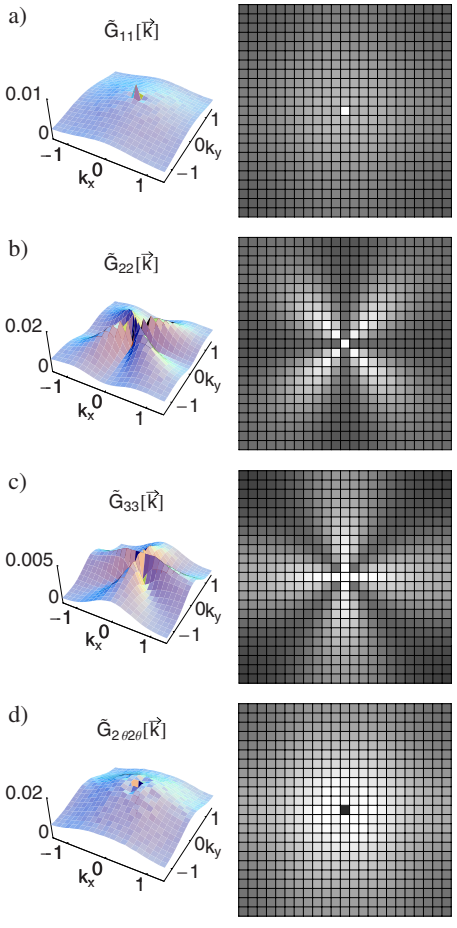

FIG. 3. (Color online) Strain-strain correlation functions of a harmonic triangular lattice at zero hydrostatic pressure as obtained from Monte Carlo simulations in the NpT ensemble with periodic boundary conditions. Results for a system with $N=3120$ particles and a spring constant $\beta a^2 f=200/\sqrt{3}$ are shown. For each function a surface plot and next to it a density plot are displayed. In the density plot the maxima are white, minima are black.

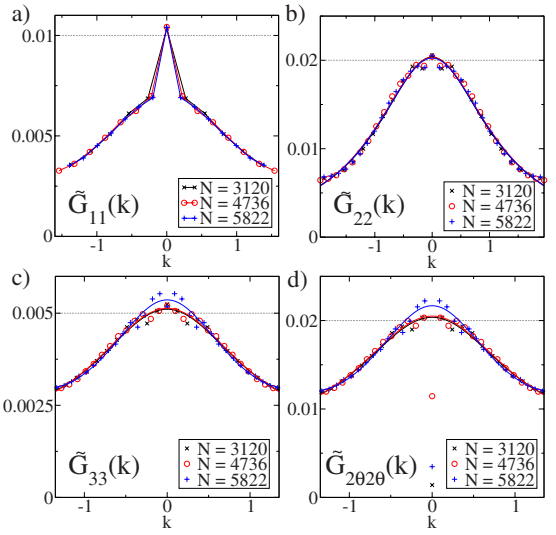

FIG. 4. (Color online) Cuts of the strain-strain correlation functions in the NpT ensemble with periodic boundary conditions at zero hydrostatic pressure along specific directions in Fourier space. (a) $\tilde{G}_{11}(\vec{k})$ along $k_y=2k_x$, (b) $\tilde{G}_{22}(\vec{k})$ along $k_x=k_y$, (c) $\tilde{G}_{33}(\vec{k})$ and (d) $\tilde{G}_{2\theta 2\theta}(\vec{k})$ along the k_y axis. For a comparison the results for different system sizes are displayed. The horizontal broken lines mark the value expected from theory for the correlation functions at $\vec{k}=\vec{0}$.

indicates that there might be excitations in the system that are not captured by the assumption of purely affine strains.

Along the cuts, for which $\tilde{G}_{22}(\vec{k})$ and $\tilde{G}_{33}(\vec{k})$ are continuous for $\vec{k}\to\vec{0}$, fitting with a generalize Lorentzian profile yields the elastic constants and the elastic correlation lengths. For the system with $N=3120$ we obtain the shear modulus as it is given in Table I and the coefficients $c_2=34.3$, $c_2'=-0.6$, $c_3=114.1$, and $c_3'=-17.6$. So the elastic correlation lengths $\xi_{el,i}\sim\sqrt{c_i}$ are approximately 6 and 11 lattice parameters, respectively.

Figure 4(d) shows cuts of $\tilde{G}_{2\theta\ 2\theta}(\vec{k})$ along the coordinate axis. One cannot obtain the elastic modulus directly from the value of $\tilde{G}_{2\theta\ 2\theta}$ at the origin in these simulations, as the system as a whole is not an embedded system and is not free to rotate. This situation is different in a solid, which is embedded in a larger volume, as will be discussed in Sec. III D

B. *NVT* ensemble with periodic boundary conditions

Below, we present simulations in the NVT ensemble with periodic boundary conditions at a reduced density of $\varrho^*=1.0$. Table II lists the elastic constants calculated with the fluctuation method given by Squire *et al.* [23]. These authors also give a formula for calculating the stress tensor. An evaluation of the data yields $\sigma_{xy}=\sigma_{yx}=0.0$ and from the trace of the stress tensor $\beta a^2 p=-\frac{1}{2}(\sigma_{xx}+\sigma_{yy})\approx 0.1$. So we verify that the simulations represent a solid at approximately zero hydrostatic pressure.

In this ensemble, the $\vec{k}=\vec{0}$ values of the correlation functions cannot be used to calculate the elastic constants directly. We are simulating an undeformed state of the crystal, thus the integral over the fluctuations of the strains over the

TABLE II. A comparison of the elastic constants as calculated from the spring constant f and as obtained by use of various methods from data of a Monte Carlo simulation of a harmonic triangular lattice in the *NVT* ensemble with periodic boundary conditions with $N=3120$ particles and spring constant $\beta a^2 f = 200/\sqrt{3}$.

	a_1	a_2	a_3
Calculated from f	$100/\beta a^2$	$50/\beta a^2$	$200/\beta a^2$
Using Squire *et al.* [23]	$97.4/\beta a^2$	$48.3/\beta a^2$	$194.8/\beta a^2$
From fits of $\tilde{G}(\vec{k}\neq\vec{0})$		$48.1/\beta a^2$	$198.2/\beta a^2$

complete simulation volume tends to zero in this ensemble. Therefore, only fits along the directions, for which the correlation functions are continuous for $\vec{k}\to\vec{0}$, give access to the elastic constants in this ensemble. As $\tilde{G}_{11}(\vec{k})$ has no such direction, the bulk modulus cannot be obtained in this way. From these considerations one expects the strain-strain correlation functions in the *NVT* ensemble to differ from those in the *NpT* ensemble for small absolute values of $\vec{k}$. Figure 5 shows surface plots and density plots of the strain-strain correlation functions in Fourier space. As in Sec. III A the anisotropies are recovered well. Only the eightfold rotational symmetry of $\tilde{G}_{11}(\vec{k})$ is not resolved. The expected discontinuous jump to $\tilde{G}_{ii}(\vec{k}=\vec{0})=0$ $(i=1,2,3)$ is clearly visible. Besides this, the correlation functions coincide with those obtained in the *NpT* ensemble. This can be seen by comparing Figs. 4 and 6, showing the same cuts in Fourier space for the various correlation functions. The elastic constants a_2 and a_3, as they are obtained from fitting the strain-strain correlation functions, are listed in Table II. They fall within 3%–4% of the theoretical values. Thus, they have the same accuracy as the values obtained via Squire's fluctuation formulas [23]. In addition the elastic correlation lengths could be obtained from the coefficients: $c_2=37.4$, $c_2'=-1.3$, $c_3=118.2$, and $c_3'=18.8$. So consistent to the results obtained from the simulations in the *NpT* ensemble $\xi_{el,i}\sim 6$ and 11 lattice parameters, respectively. Fitting e.g., $\tilde{G}_{22}(\vec{k}\neq\vec{0})$ along the direction $k_y=2k_x$ allows the determination of the coefficients $c_1=54.3$ and $c_1'=-86.1$. Correlations of volume fluctuations thus decay over approximately 7 lattice parameters. The harmonic, triangular lattice in the *NVT* ensemble was also analyzed with *open* boundary conditions. The results were discussed in detail in [13].

C. Influence of hydrostatic pressure

How does an external, hydrostatic pressure—i.e., $\sigma_{xy}=\sigma_{yx}=0$ and $\sigma_{xx}=\sigma_{yy}=-p$—influence the strain-strain correlation functions? Simulations of a harmonic, triangular lattice with spring constant $\beta a^2 f = 200/\sqrt{3}$ subjected to an external, hydrostatic pressure $\beta a^2 p = 20/\sqrt{3}$ were carried out. They show, that the shape of the correlation functions is not affected. The *NpT* ensemble was chosen for this study. Strains were calculated with respect to the average lattice positions, that is the compressed lattice. The lattice parameter of this reference lattice $a'=1.010\,465$ is smaller than the

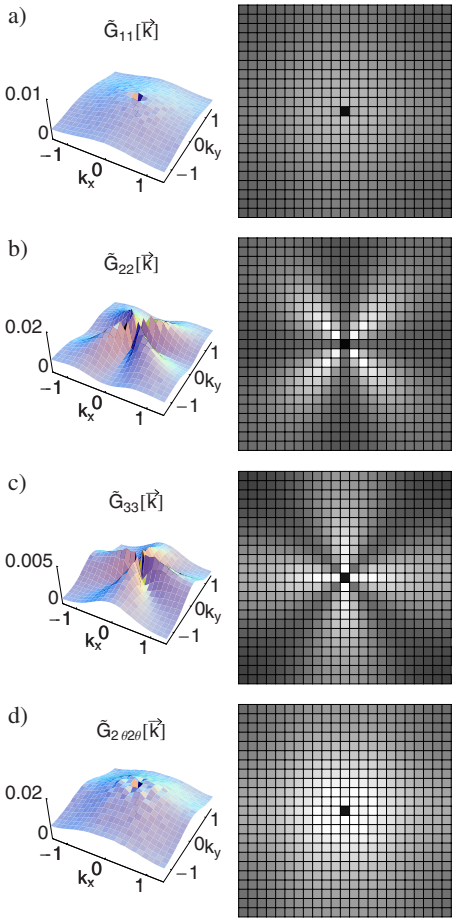

FIG. 5. (Color online) Strain-strain correlation functions of a harmonic triangular lattice as obtained from Monte Carlo simulations in the *NVT* ensemble with periodic boundary conditions. Results for a system with $N=3120$ particles and a $\beta a^2 f = 200/\sqrt{3}$ are shown. For each function a surface plot and next to it a density plot are displayed. In the density plot the maxima are white, minima are black.

lattice parameter $a=(2/\sqrt{3})^{1/2}$ in the zero-pressure simulations. Therefore, for a comparison with the theoretical values, which were given in units of βa^2, the a_i obtained from the simulation must be rescaled to these units. Simulations were run for a system with $N=3120$ particles. For a direct comparison of the correlation functions in systems with and without a hydrostatic pressure cuts in Fourier space of the $\tilde{G}_{ii}(\vec{k})$ $(i=1,2,3,2\theta)$ are shown in Fig. 7.

These show clearly the shift in the absolute values and the persistence of their shape. When relating the parameter a_i to the elastic moduli of the system, one has to recall the following. The strain-strain correlations are related to the stiffness tensor B_{ijkl}. This tensor is defined via the stress-strain relations. These relate the variation of stress to the variation of strain, to first order in the strains, for the case, that an arbitrary initial configuration $\{\vec{R}\}$ is transformed to a final configuration $\{\vec{r}\}$ by an applied uniform stress. Thus $B_{ijkl}(\{\vec{R}\}) \equiv (\partial\sigma_{ij}(\{\vec{r}\})/\partial\epsilon_{kl})_{\{\vec{R}\}} = \frac{1}{2}(\sigma_{il}\delta_{jk}+\sigma_{jl}\delta_{ik}+\sigma_{ik}\delta_{jl}+\sigma_{jk}\delta_{il}-2\sigma_{ij}\delta_{kl}) + C_{ijkl}$ [24]. The stiffness tensor explicitly depends on the applied stress. Only for the case that $\sigma_{ij}=0$ is it equivalent to

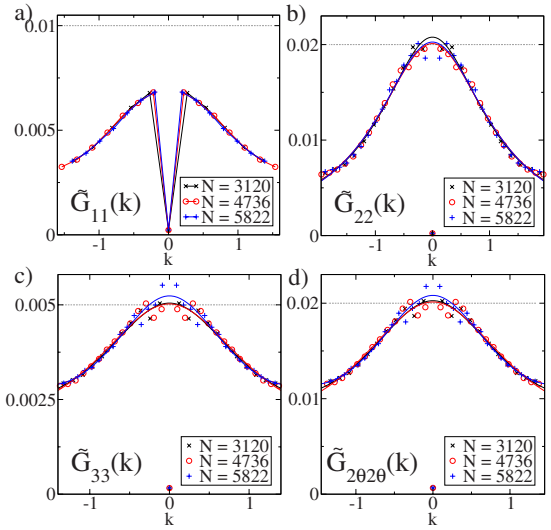

FIG. 6. (Color online) Cuts of the strain-strain correlation functions in the *NVT* ensemble with periodic boundary conditions along specific directions in Fourier space. (a) $\tilde{G}_{11}(\vec{k})$ along $k_y=2k_x$, (b) $\tilde{G}_{22}(\vec{k})$ along $k_x=k_y$, (c) $\tilde{G}_{33}(\vec{k})$ and (d) $\tilde{G}_{2\theta 2\theta}(\vec{k})$ along the k_y axis. For a comparison the results for different system sizes are displayed. The horizontal broken lines mark the value expected from theory for the correlation functions at $\vec{k}=\vec{0}$.

the tensor of the elastic constants C_{ijkl}. For the calculation of the elastic moduli the following combinations are needed:

$$\frac{1}{2}(B_{xxxx}+B_{xxyy})=\frac{1}{2}(C_{xxxx}+C_{xxyy})-\frac{1}{2}(p-p)=K,$$

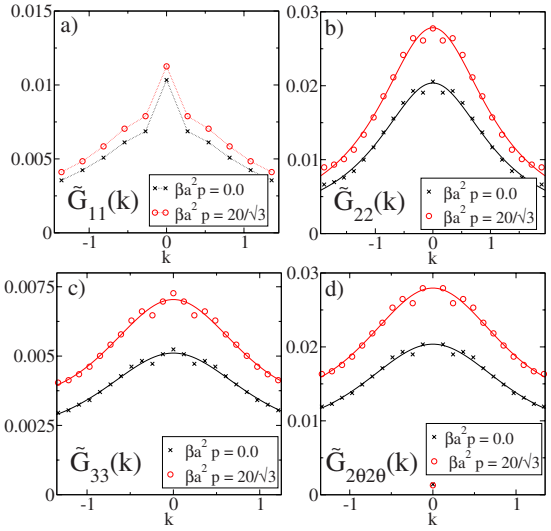

FIG. 7. (Color online) Cuts of the strain-strain correlation functions in the *NpT* ensemble with periodic boundary conditions along specific directions in Fourier space. Shown are the correlation functions obtained in a system without (crosses) external pressure and a system with $\beta a^2 p=20/\sqrt{3}$ (circles). Both systems have $N=3120$ and a spring constant $\beta a^2 f=200/\sqrt{3}$. (a) $\tilde{G}_{11}(\vec{k})$ along $k_y=2k_x$, (b) $\tilde{G}_{22}(\vec{k})$ along $k_x=k_y$, (c) $\tilde{G}_{33}(\vec{k})$, and (d) $\tilde{G}_{2\theta 2\theta}(\vec{k})$ along the k_y axis.

$$\frac{1}{2}(B_{xxxx}-B_{xxyy})=\frac{1}{2}(C_{xxxx}-C_{xxyy})-\frac{1}{2}(p+p)=\mu-p,$$

$$B_{xyxy}=C_{xyxy}-p=\mu-p.$$

Thus the bulk modulus can be directly obtained from a_1, while from $\tilde{G}_{22}(\vec{k})$ one extracts $a_2=\mu-p$ and from $\tilde{G}_{33}(\vec{k})$ one obtains $a_3=4(\mu-p)$. The values of the elastic moduli calculated according to this scheme are given in Table III. They lie within 4.4% of the theoretical values.

D. Effects of an embedding medium and finite-size

Often the strain-strain correlations cannot be evaluated over the complete crystal. In experiments as for example a two-dimensional colloidal crystal [10,13] configurational data is taken via video microscopy. Here, the area accessible to the video camera is far smaller than the complete sample size. In these cases only a subsystem embedded in a larger continuum is analyzed. As Zahn *et al.* [10] noted the presence of an infinite, embedding medium alters the relation of the strain fluctuations to the elastic moduli.

The strain-strain correlation functions are the response functions to a strain perturbation at the origin. Figure 8 shows schematically the resulting displacement field and strain fields for the cases that this perturbation is a) a dilatation and b) a rotation. The connection between the strain correlations and the elastic moduli was derived under the assumption, that the considered functional of the free energy accounts for the free energy of the complete system (equipartition theorem). For the case that the volume V_B over which the strain-strain correlation function are calculated is not equal to the complete system volume V this assumption is not fulfilled any more. As can be deduced from the schematic plots of the strain fields in Fig. 8 the energy related to the resulting strain field outside V_B cannot be neglected for $V_B \neq V$.

Following the argument by Zahn *et al.* [10], but considering a *finite* embedding continuum, we show that the influence of the surrounding medium on the strain fluctuations within the analyzed volume V_B depends on the relative size of V_B in comparison to the complete system volume V, i.e., the ratio of V_B/V. For the derivation of the formulas we consider first a homogeneous dilatation of a disk $V_B=\pi R_B^2$ in a surrounding medium of volume $V=\pi R^2$. Second we consider a pure shear, which can be realized by a rotation by an angle θ of the disk with volume V_B. For these considerations we work in polar coordinates, where we have $e_1=(\epsilon_{rr}+\epsilon_{\varphi\varphi})$, $e_2=(\epsilon_{rr}-\epsilon_{\varphi\varphi})$ and $e_3=\epsilon_{r\varphi}$. In both cases considered here it is assumed that the displacement field on the boundary of the complete system is given by $\vec{u}(\vec{r}=\vec{R}_{boundary})=\vec{0}$.

1. Homogeneous dilatation

An isotropic expansion of a disk embedded in a finite medium is given by $R_B \rightarrow R_B+\Delta r$. The resulting displacement field in polar coordinates is given by

TABLE III. The elastic moduli of the harmonic system calculated from the spring constant $\beta a^2 f = 200/\sqrt{3}$ in comparison to simulation results. Listed are the elastic constants a_i as obtained from $\tilde{G}_{ii}(\vec{k}=\vec{0})$ for a simulation in the NpT ensemble with periodic boundary conditions of a harmonic, triangular lattice with $\beta a^2 p = 20/\sqrt{3}$. For comparison with the theoretical values the a_i obtained in units of the lattice parameter a' of the compressed reference lattice have to be rescaled to the lattice parameter a of the zero-pressure reference lattice and the relation between the stiffness tensor B_{ijkl} and the tensor of elastic constants C_{ijkl} in a system with $\sigma_{ij} \neq 0$ need to be considered.

Calculated from f	$100/\beta a^2$	$\mu = a_2 + p = 50/\beta a^2$	$4\mu = a_3 + 4p = 200/\beta a^2$
From $\tilde{G}(\vec{k}=\vec{0})$	$88.8/\beta a'^2$	$a_2 = 36.0/\beta a'^2$	$a_3 = 137.6/\beta a'^2$
Rescaled values	$100.4/\beta a^2$	$a_2 = 40.7/\beta a^2 \rightarrow \mu = 52.2/\beta a^2$	$a_3 = 155.6/\beta a^2 \rightarrow 4\mu = 201.8/\beta a^2$

$$u_\varphi = 0, \quad u_r = \begin{cases} \Delta r \dfrac{r}{R_B} & \text{for} \quad r < R_B \\ \Delta r \dfrac{R_B}{r} & \text{for} \quad r > R_B. \end{cases}$$

From this it is straight forward to calculate the resulting strain field and consequently the Free Energy density $f = \frac{1}{2}[K(\epsilon_{rr}+\epsilon_{\varphi\varphi})^2 + \mu((\epsilon_{rr}-\epsilon_{\varphi\varphi})^2 + 4\epsilon_{r\varphi}^2)]$ of the system under load. Thus the total energy needed for such an expansion in a finite system of volume $V = \pi R^2$ is given by $E = \int_0^{2\pi}\int_0^R r d\varphi dr f = (V_B/2)(\Delta V_B/V_B)^2\{K + \mu[1-(V_B/V)]\}$. For such a system equipartition tells us thus, that the strain fluctuations are no longer set by the bulk modulus of the system, but acquire in the embedded system a term dependent on the shear modulus *and* on the ratio V_B/V:

$$\frac{k_B T}{V_B}\langle e_1^2 \rangle = \frac{1}{K + \mu\left[1 - \left(\dfrac{V_B}{V}\right)\right]}.$$

Therefore the strain-strain correlation function $G_{11}(\vec{r})$ no longer provides access to the bulk modulus, but to a V_B/V-dependent combination of bulk and shear modulus.

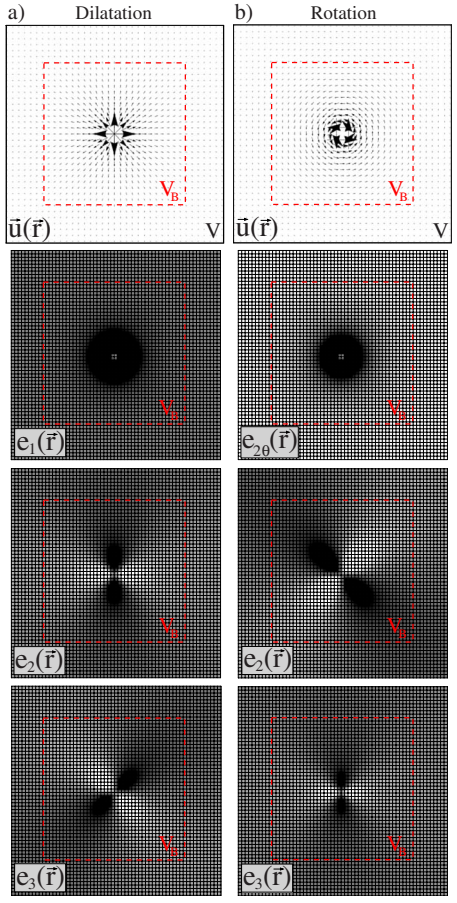

FIG. 8. (Color online) A schematic drawing of the displacement field $\vec{u}(\vec{r})$ and below the corresponding strain fields as they result from a given perturbation at the origin: (a) a dilatation and (b) a rotation a the disk at the origin. If the analyzed volume V_B (broken red line) does not coincide with the volume of the complete system V (black line), the energy needed for the displacements in the embedding medium $(V-V_B)$ must be taken into account in the interpretation of the correlation functions.

2. Pure shear

A rotation of the disk as a rigid body within the embedding medium by an infinitesimal angle $\Delta\varphi$ changes a given orientation φ to $\varphi+\Delta\varphi$. The resulting displacement field is given by

$$u_r = 0, \quad u_\varphi = \begin{cases} 0 & \text{for} \quad r < R_B \\ \Delta\varphi \dfrac{R_B^2}{r} & \text{for} \quad r > R_B. \end{cases}$$

From the corresponding strain field the free-energy density can be determined and integration over the complete system yields the energy required for such a rotation: $E = \mu(2\Delta\varphi)^2 V_B(1-(V_B/V))/2$. In case of infinitesimal rotation angles $\Delta\varphi$ this angle can be identified with the antisymmetric part of the strain tensor $\theta = (\partial u_y/\partial x - \partial u_x/\partial y)/2$. Equipartition relates the fluctuations in $e_{2\theta}$ to the shear modulus μ:

$$\frac{k_B T}{V_B}\langle e_{2\theta}^2 \rangle = \frac{1}{\mu\left[1 - \left(\dfrac{V_B}{V}\right)\right]}.$$

The obtained relation also depends on V_B/V. This is consistent with the fact, that the energy required for the rotation of a disk, which is not embedded in a surrounding medium $(V_B \rightarrow V)$, tends to zero. The analysis of the strain variable 2θ offers thus an independent, direct route to the determination of the shear modulus in an embedded system.

These considerations show that in order to obtain accurate elastic moduli from the analysis of the strain fluctuations the

relative size of the analyzed system to the complete, finite system should to be known. Nevertheless for the case of the colloidal crystal [13] the situation is close to the limiting case of $\frac{V_B}{V} \to 0$. Here, the influence of the surrounding medium on the analyzed system is dominant. The strain variables e_1 and $e_{2\theta}$ can be used to extract the elastic moduli. Thus the two-dimensional colloidal crystal, as discussed in detail in [13,19] is an example for a completely embedded system. In contrast to this in simulations the complete system can be analyzed, which corresponds to the limiting case of $\frac{V_B}{V} \to 1$. For this case each of the strain-strain correlation functions of the strain variables e_1, e_2, and e_3 give directly access to the corresponding elastic moduli a_i. The effect of the embedding medium can be visualized by looking at a statistical sum rule, as will be discussed in the next paragraph.

3. Analysis of a statistical sum rule

The sum rule for the generalized susceptibility provides another way of extracting the elastic moduli from the strain-strain correlation functions. The coarse-grained system represents a homogeneous continuum and is thus translationally invariant. For such systems the susceptibilities are directly related to the correlation functions. In Fourier space this reads $\tilde{\chi}_T(\vec{k}) = \beta \tilde{G}(\vec{k})$. From this the static susceptibility sum rule follows [18]:

$$\chi_T = \lim_{\vec{k} \to \vec{0}} \tilde{\chi}_T(\vec{k}) = \beta \tilde{G}(\vec{k})|_{\vec{k}=\vec{0}} = \beta \int d\vec{r} G(\vec{r}).$$

Thus an integration of the correlation functions in real space yields directly the generalized susceptibilities χ_T. Here, these correspond to the elements of the compliance tensor S_{ijkl}. The compliance tensor is the inverse of the stiffness tensor B_{ijkl}. In the case that *no* external stresses act on the system this is equivalent to the tensor of the elastic constants C_{ijkl} [24]. The S_{ijkl} obtained from such an analysis depend on the integration volume V_B. Thus in order to obtain systems-size independent values an additional finite-size scaling analysis should be employed.

Figure 9 shows the compliances S_{ii} ($i=1$, 2, 3, and 2θ) as a function of the ratio of the integration volume V_B to the complete simulation volume V, i.e., $V_B/V = L_B/L$. These were obtained from the simulation data of the harmonic triangular crystal at zero external pressure in the NpT and NVT ensemble with different boundary conditions. A comparison shows directly how the choice of ensemble and the choice of boundary conditions influences the results. These are so called explicit and implicit finite-size effects [25]. In addition this analysis visualizes the effects of the embedding medium on the compliances S_{ii}.

Figure 9(a) shows the results from simulations in the NpT ensemble with periodic boundary conditions. The complete system contains $N=5822$ particles connected via springs of spring constant $\beta a^2 f = 200/\sqrt{3}$. The strain-strain correlation functions are directly related to the elastic moduli in this ensemble, due to the fact that the volume itself fluctuates. Thus one can obtain the elastic moduli directly from the S_{ii} at $L_B/L=1$. For the considered system we find: $S_{11}^{(L)}=0.01025$, $S_{22}^{(L)}=0.02050$, $S_{33}^{(L)}=0.00512$, and $S_{2\theta 2\theta}^{(L)} \to 0$, resulting in $a_1=97.5$, $a_2=48.7$ and $a_3=195.2$. These values lie within 2.5% of the expected values. The accuracy of this approach compares to that of the methods for the calculation of the elastic moduli discussed before. From the considerations in Sec. III D 1 one expects the following functional dependence of S_{11} on L_B/L:

$$S_{11}^{(L_B)} = V_B \langle e_1^2 \rangle / (k_B T) = \{K + \mu[1 - (L_B^2/L^2)]\}^{-1}.$$

The black solid line in Fig. 9(a) is a fit with this equation to the data (crosses). From the fit parameters the following elastic moduli are extracted: $a_1=K=93.4$ and $\mu=a_2=45.8$. Figure 9(a) shows clearly the increasing impact the surrounding medium has on S_{11} as L_B/L diminishes. In the limit $V_B/V \to 0$ it yields the sum of the elastic moduli K and μ. It is apparent from Fig. 9(a), that as soon as $V_B/V < 1$, the com-

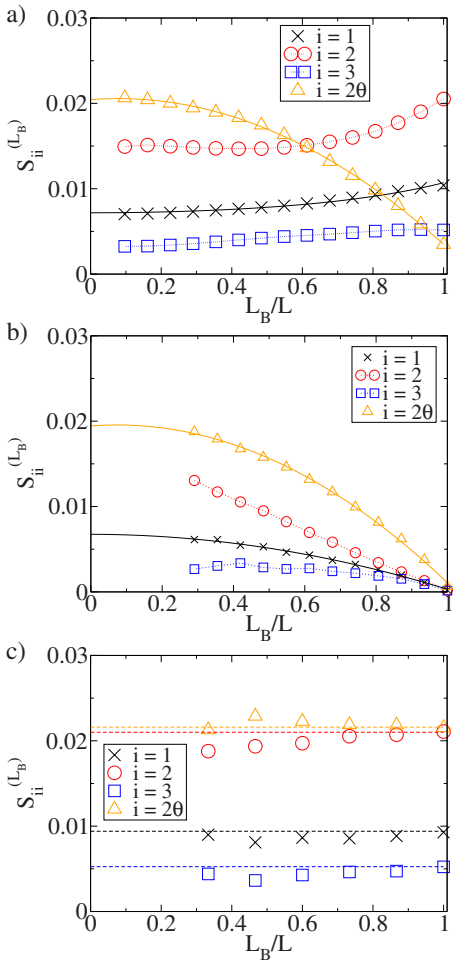

FIG. 9. (Color online) Compliances S_{ii} as they are obtained from the sum rule as a function of the ratio of analyzed volume $V_B=L_B^2$ to the complete simulation volume $V=L^2$. Shown are the results of Monte Carlo simulations of a harmonic triangular lattice with $N=5822$ particles and spring constant $\beta a^2 f = 200/\sqrt{3}$. Lines are a fit to the data with the formulas given in the text, while the dotted lines are a guide for the eyes. (a) NpT ensemble with periodic boundary conditions. (b) NVT ensemble with periodic boundary conditions. (c) NVT ensemble with open boundary conditions. Here dashed lines show the value for $L_B/L=1$ as a comparison.

pliances S_{22} and S_{33} cannot be directly related to the shear modulus any more.

The considerations in Sec. III D 2 suggest, that the compliance $S_{2\theta 2\theta}$ should diverge as $V_B/V \to 1$. This relates to the fact, that the energy needed for rotating an embedded disk goes to zero as the embedding material is removed. This divergence cannot be seen in the simulation data. In simulations with periodic boundary condition the system as a whole cannot rotate. The fact, that there is no divergence of $S_{2\theta 2\theta}$ for $V_B/V \to 1$, is therefore an implicit finite-size effect. In order to extract the shear modulus from the compliance $S_{2\theta 2\theta}$ a polynomial in (L_B/L) was fitted to the data (open triangles). From the limit $V_B/V \to 0$ the shear modulus is extracted: $\mu = 48.9$.

In the *NVT* ensemble with periodic boundary conditions the compliances as a function of L_B/L exhibit a different dependence on L_B/L, as Fig. 9(b) shows. An unstrained state of the triangular lattice is analyzed in these simulations. Thus, the integral of the correlation functions over the complete system goes to zero and gives no access to the elastic moduli. This is an explicit finite-size effect. Nevertheless from the limit $V_B/V \to 0$ one can extract the elastic moduli as in the case of the simulations in the *NpT* ensemble with periodic boundary conditions from the compliances S_{11} (crosses) and $S_{2\theta 2\theta}$ (open triangles). Fits with a polynomial in (L_B/L) are plotted as solid lines in Fig. 9(b). From the case of maximum embedding one extracts $a_1 + a_2 = K + \mu = 148.3$ from S_{11} and $a_2 = 51.5$ from $S_{2\theta 2\theta}$ in Fig. 9(b). These values compare to the values obtained by different methods as they are given in Table II.

The compliances $S_{ii}^{L_B}$ shown in Fig. 9(c) are obtained from data of simulations in the *NVT* ensemble with open boundary conditions as they were presented in [13]. These show in contrast no systematic dependence on V_B/V. The maximum analyzed volume, which will for this case be denoted by $V = L^2$, is approximately one fourth of the complete system volume. In this case the averaging over the positions of origin results in an averaging over subsystems with partial to complete embedding. For this type of averaging the $\vec{k} = \vec{0}$ values of *all* considered strain-strain correlation functions give access to the elastic moduli of the system [13]. The effect of this type of averaging shows up most prominently in the fact that $S_{2\theta 2\theta}$ does not tend to zero for $L_B/L \to 1$, but approaches the value of S_{22}. Extracting the elastic moduli from the compliances for $L_B/L = 1$ in Fig. 9(c) yields $S_{11}^{(L)} = 0.009\,40 \to a_1 = 106.9$, $S_{22}^{(L)} = 0.021\,00 \to a_2 = 47.6$, $S_{33}^{(L)} = 0.005\,25 \to a_3 = 190.4$ and $S_{2\theta 2\theta}^{(L)} = 0.021\,60 \to a_2 = 46.4$. The accuracy of these values is the same as in [13]. The deviation from the theoretical values is larger in this case, as the finite system with open boundary conditions is influenced in its elastic properties by the missing stabilizing bonds for particles at the surfaces.

IV. STATISTICS OF NONAFFINE FLUCTUATIONS

The comparison between the analytic predictions for the strain-strain correlation functions (Figs. 1 and 2) and those obtained from the coarse-graining procedure on the simulation data (e.g., Figures 3 and 4) shows that the analytically predicted discontinuities are reduced. Here we demonstrate that the source of these deviations from the analytic predictions is a nonaffine noise field present in the simulations as well as in experimental data. Nonaffine fluctuations are not included in our Landau ansatz for the Free Energy functional. The ansatz was based on the assumption of purely affine strains e_i. There are two sources of nonaffine contributions. In the crystal short-wavelength excitations might occur, which could lead to the formation of defects. Far away from the melting point these contributions are not dominant. In addition to these fluctuations, the coarse-graining procedure described in Sec. III, which is employed in the data analysis, also contributes.

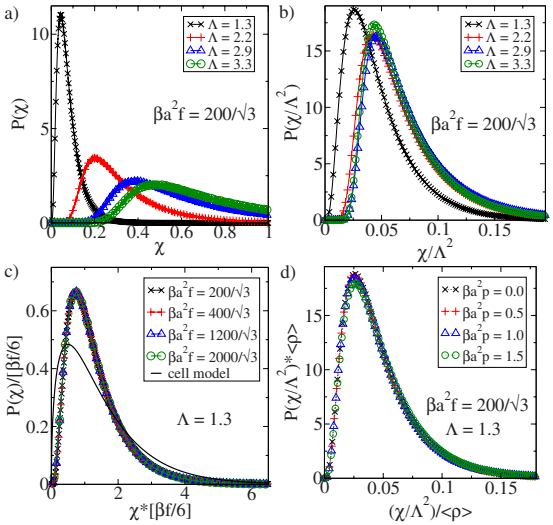

FIG. 10. (Color online) Plots of the probability distribution of the nonaffinity parameter χ from simulations in the *NpT* ensemble with periodic boundary conditions and $N = 3120$ particles. (a) Plot of the probability distribution of $P(\chi)$ vs χ for various coarse-graining length Λ. (b) The probability distribution of χ/Λ^2 shows a data collapse for $\Lambda \geq 2.2$. (c) Data for various spring constants f collapse onto each other. The prediction from a simple cell model (black line) is shown for comparison. (d) Data from simulations at various hydrostatic pressure p scale with the resulting average density $\langle \varrho \rangle$.

It projects the configurations generated by our microscopic Hamiltonian onto strain fields, which are smooth over distances larger than the coarse-graining length Λ. It also generates a conjugate noise [14]. This noise represents those fluctuations, which cannot be captured during coarse-graining. In order to understand this one has to realize the following. Coarse-graining retains only that part of the particle displacements $\vec{u} = \vec{r} - \vec{R}$ in a configuration, which can be obtained from the reference lattice $\vec{R}$ by an affine transformation: $\vec{r} = (\mathbf{1} + \epsilon)\vec{R}$. An affine transformation constrains all parallel lines in the reference lattice to remain parallel. This is clearly impossible to satisfy for an arbitrary configuration coarse-grained over volumes larger than an unit cell. Indeed, the quantity χ as defined in Eq. (7) has the dimension of Length^2 and scales as Λ^2. This may be seen by comparing Figs. 10(a) and 10(b). Figure 10 shows the probability distribution $P(\chi)$ and its scaling behavior for various choices of parameters. While Fig. 10(a) shows a clear dependence of the amount of nonaffinity on the coarse-graining length Λ,

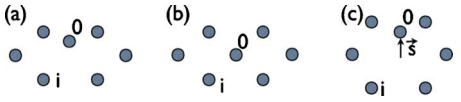

FIG. 11. (Color online) Example configuration (a) consisting of a central particle 0 and neighboring particles $i=1,6$ which can be decomposed into a purely affine deviatoric distortion (b) together with a nonaffine displacement $\vec{s}$ of the central particle 0 (c).

Fig. 10(b) shows a collapse of the distributions for the scaled quantity χ/Λ^2 for $\Lambda>2.2$. This corresponds to a minimum of 18 neighbors to the central particle, that are taken into account in the calculation of the strain field via the minimization of χ. These distributions show a constant offset from $\chi/\Lambda^2=0$. By contrast $\Lambda=1.3$ shows no such offset. This means that for the calculation of the affine strain field only the minimal neighborhood, i.e., the 6 nearest neighbors, allows for a global minimization of χ. In addition the probability distributions of the nonaffine parameter χ also scale with the spring constant f [Fig. 10(c)] and in simulations run at various hydrostatic, external pressure p with the resulting average density $\langle\varrho\rangle$ [Fig. 10(d)]. One can therefore obtain the probability distribution for χ for any inverse temperature β, spring constant f, density ρ and coarse-graining length Λ from a generalized extreme value probability distribution function. This master curve is $P(\mathcal{X})=((1+0.27\cdot z)^{(-1/0.27)-1}e^{-(1+0.27\cdot z)^{-1/0.27}})/2.012$ with $z=(\mathcal{X}-3.127)/2.012$, which we obtain from a fit to the simulation data with the scaling variable $\mathcal{X}=\chi\beta f/\rho\Lambda^2$. The scaling was found to be independent of system size N and the choice of ensemble.

We show below that features of $P(\chi)$, like the dependence on the spring constant f, may be rationalized within a simple "cell model" calculation. In this model each particle is assumed to fluctuate within the cage of its 6 nearest neighbors which suffers, at most, an affine distortion (see Fig. 11). The only source of nonaffinity comes from the displacement of the central particle from its equilibrium position.

For such a subset of configurations, one may simply decompose each configuration $\{\vec{r}\}$ into one obtained by an affine transformation plus a nonaffine displacement $\vec{s}$ of the central particle within an undistorted hexagonal cell. The nonaffinity parameter χ may then be calculated to be

$$\chi=\sum_{m=1}^{6}\sum_{i=1}^{2}\left\{r_m^i-r_0^i-\sum_{j=1}^{2}(\delta_{ij}+\epsilon_{ij})(R_m^j-R_0^j)\right\}^2$$
$$=\sum_{m=1}^{6}\sum_{i=1}^{2}[r_m^i-r_0^i-(R_m^i-R_0^i)]^2=6s^2.$$

Within this approximation the ensemble average $\langle\chi\rangle$ contributes to the Lindemann parameter l. This is due to the fact, that the fluctuations of the displacement field can be related to the Lindemann parameter as follows: $\langle|u|^2\rangle=\langle(\vec{u}_{\text{affine}}+\vec{s})^2\rangle=\langle u_{affine}^2\rangle+\langle\chi\rangle/6+2\langle|u_{\text{affine}}|*|s|\rangle=l^2a^2$. The Lindemann ratio depends on the stiffness of the solid and grows as the melting point is approached. In order to calculate $P(\chi)$ within this simple "cell model," we first calculate the energy of such a "cell" configuration:

$$E=\frac{f}{2}\sum_{i=1}^{6}(|\Delta\vec{R}_i-\vec{s}|-|\Delta\vec{R}_i|)^2$$
$$=\frac{f}{2}\sum_i\{2\Delta\vec{R}_i^2+\vec{s}^2-2\vec{s}\cdot\Delta\vec{R}_i$$
$$-2\Delta\vec{R}_i^2\sqrt{1+\vec{s}^2/\Delta\vec{R}_i^2-2\Delta\vec{R}_i\cdot\vec{s}/\Delta\vec{R}_i^2}\}\approx 3fs^2.$$

Here we used an approximation of the square root up to $\mathcal{O}(4)$ and the abbreviation $\Delta\vec{R}_i=\vec{R}_i-\vec{R}_0$. Thus the energy related to the nonaffinity χ of the central particle is $E_{cell}=E/3=f\chi/6$. With this energy contribution it is straight forward to calculate the probability distribution of χ,

$$P(\chi)=C\int d\vec{s}e^{-\beta fs^2}\delta(\chi'(s)-\chi)=\frac{2}{\sqrt{\pi}}\left(\frac{\beta f}{6}\right)\phi^{1/2}e^{-\phi}, \quad (8)$$

where $\phi=\frac{\beta f}{6}\chi$ and C, the normalization constant. In Fig. 10(c), we have plotted $P(\chi)/(\beta f/6)$ from this cell model together with the scaled distributions obtained from our simulations. The data collapse of the distributions from simulations with various spring constants is in accord with the scaling in $\beta f/6$ as expected from the simple cell model. The details of the shape of the distribution function cannot be captured completely. As is to be expected in this simple model, the contributions of large χ are slightly overestimated.

How does the presence of χ influence strain correlations? To see this we assume that, at least for small χ the total strain obtained by fitting an arbitrary configuration to an affine transformation can be decomposed into two parts. An affine part, which would have been the only result, if χ were zero, and a χ dependent, nonaffine part. This nonaffine part may be expanded as a series in powers of χ. Thus we assume

$$\epsilon_{ij}(\chi;\vec{r})=\epsilon_{ij}^0(\vec{r})+\sum_p t_p\chi(\vec{r})^p.$$

This decomposition is more general than the assumption of purely affine strains. To lowest order in χ the strain correlations can, therefore, be written as

$$\langle\epsilon_{ij}(\chi;0)\epsilon_{kl}(\chi;\vec{r})\rangle=\langle\epsilon_{ij}^0(0)\epsilon_{kl}^0(\vec{r})\rangle+t_1^2\langle\chi(0)\chi(\vec{r})\rangle.$$

Here, we have used the fact, that the coarse-graining process projects the displacements into mutually orthogonal subsets [14,26]. Thus, one can ignore all correlations between ϵ_{ij}^0 and χ. So we see that the correlations of the nonaffinity, i.e., $G_{\chi\chi}(\vec{r})=\langle\chi(0)\chi(\vec{r})\rangle$, will alter the strain-strain correlations. In Fig. 12(a), we have plotted cuts showing the decay of $G_{\chi\chi}(\vec{r})$ along the x and y axis. The function $G_{\chi\chi}$ is isotropic and decays rapidly to zero over a length scale comparable to Λ. This suggests that χ behaves as a "delta" correlated white noise with a probability distribution given by Eq. (8). This is consistent with our identification of χ with the Lindemann ratio. The microscopic, random, thermal fluctuations of individual particles are, indeed, expected to be uncorrelated with each other. Given the form of $G_{\chi\chi}$ one expects such fluctuations to contribute a background term [compare Fig. 12(b)] to the strain correlations in Fourier space. This explains the deviation of the strain-strain correlation functions $\tilde{G}_{ii}$ ob-

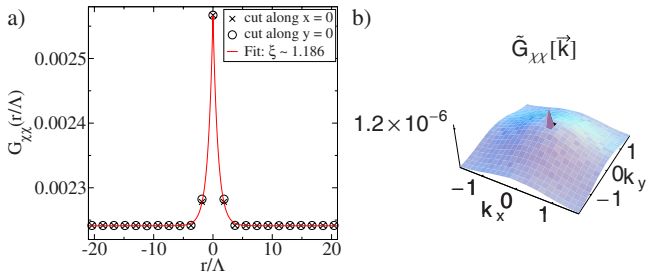

FIG. 12. (Color online) (a) The autocorrelation function of the nonaffinity parameter χ for the harmonic triangular lattice with spring constant $\beta a^2 f = 200/\sqrt{3}$ in the NpT ensemble with periodic boundary conditions along the x and the y axes. The red line is a fit to an exponential form. (b) A surface plot of its Fourier transform $\tilde{G}_{\chi\chi}(\vec{k})$.

tained from simulation data from the predicted analytic form. The $\tilde{G}_{ii}$ obtained from simulation data retain a weak dependence on the coarse-graining length Λ. As Λ is set larger the elastic moduli $a_i = 1/\tilde{G}_{ii}(\vec{k}=\vec{0})$ take on higher values, while the correlation lengths $\sqrt{c_i}$ diminish. This is consistent with the smoothening out of displacement fluctuations with longer and longer wavelength with increasing Λ and corresponds to a situation, where the crystal is shifted to lower temperatures. On the other hand a numerical extrapolation to $\Lambda \to 0$ gives slightly improved values for the elastic constants $a_i = 1/\tilde{G}_{ii}(\vec{k}=\vec{0})$.

We have shown in this section that the coarse-graining process by which affine strains may be extracted from microscopic particle configurations also generates a random white noise consisting of nonaffine particle displacements. For a harmonic solid this is simply related to the Lindemann parameter. This, in turn, depends ultimately on the strength of the interactions.

What is the general implication of this to the study of elasticity and rheology of complex solids? The current picture of the mechanism of relaxation in amorphous materials indicates that there are two main competing processes involved [27]. Over small time scales the system fluctuates within local minima in the free energy landscape. Transition between such basins of attraction occur only over longer time scales. We have shown here that harmonic fluctuations within local minima generate a well characterized contribution to the nonaffinity χ. This means, that any "extra" contribution to χ arises exclusively from these interbasin transitions. Thus our analysis may be used as a tool to distinguish between these two kinds of relaxations in complex solids.

V. CONCLUSIONS

We have shown in this paper how the analysis of particle configurations of two-dimensional soft solids gives access to a wealth of information on the local and nonlocal elastic properties. Since the harmonic solid analyzed here is the most generic conceivable, our work has the potential to serve as a template for further research in this direction. The properties of the strain-strain correlation functions have been discussed in great detail and various methods of how to extract the elastic moduli from their analysis were presented. Furthermore we determined and discussed the effects of external pressure and an embedding medium. The proper treatment of the latter is essential for experimentalists seeking to use our methods for analyzing mechanical behavior of soft matter. The implications of our work particularly for the understanding of nonaffineness in solids is significant, because our study allows one to classify nonaffine fluctuations in any system into "trivial" (in the sense of being present even in an ideal harmonic solid) and nontrivial components. In the future, we shall use these procedures to study metastability in solids undergoing phase transitions and plastic behavior of solids under large external stresses.

ACKNOWLEDGMENTS

We acknowledge useful discussions with K. Binder, R. Messina, and M. Rao. This work was funded by the Deutsche Forschungsgesellschaft (Grant No. SFB TR6/C4). Granting of computer time from HLRS, NIC, and SSP is gratefully acknowledged. One of us (S.S.) thanks the DST, Government of India for support.

[1] A. Yethiraj and A. van Blaaderen, Nature (London) **421**, 513 (2003).
[2] P. Habdas and E. R. Weeks, Curr. Opin. Colloid Interface Sci. **7**, 196 (2002).
[3] K. J. Strandburg, Rev. Mod. Phys. **60**, 161 (1988); **61**, 747 (1989).
[4] S. Sengupta, P. Nielaba, and K. Binder, Phys. Rev. E **61**, 6294 (2000).
[5] K. Binder, S. Sengupta, and P. Nielaba, J. Phys.: Condens. Matter **14**, 2323 (2002).
[6] H. H. von Grünberg, P. Keim, K. Zahn, and G. Maret, Phys. Rev. Lett. **93**, 255703 (2004).
[7] I. Doghri, *Mechanics of Deformable Solids* (Springer, New York, 2000).
[8] A. Wille, F. Valmont, K. Zahn, and G. Maret, EPL **57**, 219 (2002).
[9] S. Sengupta, P. Nielaba, M. Rao, and K. Binder, Phys. Rev. E **61**, 1072 (2000).
[10] K. Zahn, A. Wille, G. Maret, S. Sengupta, and P. Nielaba, Phys. Rev. Lett. **90**, 155506 (2003).
[11] R. Maranganti and P. Sharma, Phys. Rev. Lett. **98**, 195504 (2007); J. Mech. Phys. Solids **55**, 1823 (2007).
[12] K.-Q. Zhang and X. Y. Liu, Langmuir **25**, 5432 (2009).
[13] K. Franzrahe, P. Keim, G. Maret, P. Nielaba, and S. Sengupta, Phys. Rev. E **78**, 026106 (2008).
[14] P. M. Chaikin and T. C. Lubensky, *Principles of Condensed Matter Physics* (Cambridge University Press, Cambridge, England, 1995).

[15] R. A. Cowley, Phys. Rev. B **13**, 4877 (1976); F. Falk, Z. Phys. B **51**, 177 (1983); A. E. Jacobs, Phys. Rev. B **31**, 5984 (1985); G. R. Barsch and J. A. Krumhansl, Metall. Trans. A **19A**, 761 (1988); R. J. Gooding and J. A. Krumhansl, Phys. Rev. B **38**, 1695 (1988); S. Kartha, J. A. Krumhansl, J. P. Sethna, and L. K. Wickham, *ibid.* **52**, 803 (1995); T. Lookman, S. R. Shenoy, K. Ø. Rasmussen, A. Saxena, and A. R. Bishop, *ibid.* **67**, 024114 (2003); A. Paul, J. Bhattacharya, S. Sengutpa, and M. Rao, J. Phys.: Condens. Matter **20**, 365211 (2008); M. Porta, T. Castan, P. Lloveras, T. Lookman, A. Saxena, and S. R. Shenoy, Phys. Rev. B **79**, 214117 (2009); A. Paul, S. Sengupta, and M. Rao, in *Proceedings of ICOMAT 08* (TMS Proceedings, USA, 2010) e-print arXiv:1003.3369.

[16] D. G. B. Edelen, in *Continuum Physics 4*, edited by A. C. Eringen (Academic, New York, 1976).

[17] M. Baus and R. Lovett, Phys. Rev. Lett. **65**, 1781 (1990); Phys. Rev. A **44**, 1211 (1991).

[18] N. Goldenfeld, *Lectures on Phase Transitions and the Renormalization Group* (Westview, Boulder, CO, 1992).

[19] K. Franzrahe, P. Nielaba, A. Ricci, K. Binder, S. Sengupta, P. Keim, and G. Maret, J. Phys.: Condens. Matter **20**, 404218 (2008).

[20] P. Keim, G. Maret, U. Herz, and H. H. von Grünberg, Phys. Rev. Lett. **92**, 215504 (2004).

[21] M. L. Falk and J. S. Langer, Phys. Rev. E **57**, 7192 (1998).

[22] M. Parrinello and A. Rahman, J. Chem. Phys. **76**, 2662 (1982).

[23] D. R. Squire, A. C. Holt, and W. G. Hoover, Physica (Amsterdam) **42**, 388 (1969).

[24] D. C. Wallace, *Thermodynamics of Crystals* (Dover, New York, 1998).

[25] F. L. Román, J. A. White, and S. Velasco, J. Chem. Phys. **107**, 4635 (1997); F. L. Román, J. A. White, A. González, and S. Velasco, *ibid.* **110**, 9821 (1999).

[26] H. Mori, Prog. Theor. Phys. **33**, 423 (1965).

[27] *Relaxations in Complex Systems*, edited by K. L. Ngai and G. B. Wright (NRL, Washington, D.C., 1985).